Preprints.org

Article

Understanding the Characteristics of Vertical Structure for Wind Speed Observation via Wind-LIDAR in Jeju Island

Dong-won Yi [*] , Sang-Sam Lee , Hee-Wook Choi , Yong Hee Lee

Article

Understanding the Characteristics of Vertical Structure for Wind Speed Observation via Wind-LIDAR in Jeju Island

Dong-Won Yi *, Sang-Sam Lee, Hee-Wook Choi and Yong Hee Lee

Department of Research Applications, National Institute of Meteorological Sciences,
Jeju 63568, Republic of Korea
* Correspondence: dwyi@korea.kr

Abstract: The wind observations for multiple levels (40–200 m) have been conducted for a long time (2016–2020) on Jeju Island of South Korea. This study aims at understanding the vertical and temporal characteristics of lower atmosphere. Jeju Island is a region located at mid-latitude and is affected by seasonal monsoon wind. The maximum wind speed appears in the lower layer during day time and is delayed in the upper layer after sunset in diurnal cycle. In summer season, the surface layer increases up to 160 m during day time via dominant solar radiation effect, which is higher than those for other seasons. However, the maximum wind speed in winter season appears irregularly among altitudes, and the surface layer is ~100 m, which is lower than that in summer season. It can be attributed to the increase in the mean wind speed in diurnal cycle caused by the strong northwestern wind for winter season. These results imply that the relationship between near-surface and higher altitudes is primarily affected by solar radiation and seasonal monsoon winds. These results are expected to contribute to site selection criteria for wind farms and to the assessment concerning planetary boundary layer modeling.

Keywords: Wind-LIDAR; multiple-level winds; diurnal cycle; atmospheric boundary layer; maximum wind speed

1. Introduction

With acceleration of global warming, the demand for renewable energy that generates eco-friendly and clean energy, such as wind power, with reduced carbon emissions is gradually increasing [1–3]. Generally, wind power–generating turbines are located within the surface layer (SL), which corresponds to ~10% of the lower layer of the atmospheric boundary layer (ABL); SL is further classified into inertial and roughness sublayers, which interact with the land surface [4]. Additionally, two layers adjacent to SL, the mixed layer (ML) and nocturnal stable boundary layer (NL), take turns developing throughout the course of days. During days, ML develops up to several kilometers owing to strong convection associated with solar radiation, whereas after sunset, with decreasing convection within ABL, ML is replaced by NL until sunrise. Concerning solar radiation, heat and momentum are exchanged within SL during days and nights, and these characteristics are also closely related to atmospheric movement and calculation of wind power generation [5]. However, processes occurring within ABL are still not properly understood [6,7]. Therefore, properly understanding the role of the lower atmospheric layer in wind power generation as a renewable energy is crucial [8]. Additionally, although various studies have been conducted on the effect of wind environment on wind power generation in lower atmospheric layers including SL [9–12], long-term observation and research on vertical wind are insufficient.

Wind light detection and ranging (Wind-LIDAR) equipment is a state-of-the-art technology for obtaining wind measurements, which has developed rapidly over the decades following the invention of the laser in 1960 [13–21]. However, limitations including low spatial resolution and inability to address local climate characteristics that considerably impact wind peak and ramp predictions still remain [22]. To overcome these limitations, ground-based remote observation

equipment, such as Wind-LIDAR, was recently introduced for climate research [23]. Wind-LIDAR can remotely measure atmospheric winds and has a higher resolution compared with existing SODAR (Sonic Detection and Ranging) [24]. Although existing observation towers installed on the ground are limited in terms of height for wind resource estimation and vertical wind observation and require high installation costs, remote observation equipment such as Wind-LIDAR has advantages in that it is easy to move and install and is cost-effective; moreover, its height settings can be conveniently changed. In this context, the National Institute of Meteorological Sciences has conducted intensive and long-term Wind-LIDAR observation at a point in the northern part of Jeju Island, which includes a section with an altitude of 40–200 m where changes in SL can also be examined. The relevant observatory has been operated to select the location of wind power plants and evaluate the environment, which facilitates provision of data on the analysis of vertical wind characteristics of the lower atmospheric layer including SL, under the circumstance where long-term vertical observation data is rare. Therefore, this study intends to investigate the vertical structure and temporal variability characteristics of wind in the lower atmospheric layer, including SL, using long-term observation data on vertical wind. The sections of this paper consist of Section 2, which introduces data collected from observation equipment and analysis methods, Section 3, presenting monthly and daily variation characteristics of vertical wind, and Section 4, including the summary and discussion.

2. Data and Methods

The long-term vertical wind observations were conducted at the Bonggae (BG) Observatory in northern Jeju-si, Jeju-do, located at ~351 m above sea level (Figure 1). The equipment used for vertical wind observation is Wind-LIDAR (by Leosphere) (33.4621°N, 126.6289°E), which is a technology applied in various fields to measure distance to objects and speed using a laser and has been reported to be more reliable than conventional remote equipment such as SODAR [25]. In the surrounding environment where the observation equipment was installed, gentle slopes were generally spread out; therefore, the influence of turbulence due to high obstacles was relatively small. The observation altitude ranged from 40 m to 200 m, with 10 layers of vertical resolution at intervals of 10 m at altitudes of ≤60 m and 20 m at altitudes >60 m; moreover, a 10-min average time resolution was calculated for each wind direction and wind speed. Observations were conducted for approximately five years from September 2016 to July 2020, and quality control of all data collected over a long time was performed according to the Meteorological Observations Standardized Manual [26]; the step test was applied to examine the maximum change (10 ms^{-1}) allowed for each observation period (10 min), followed by a test examining the minimum change (0 ms^{-1}, 0 degree) allowed for continuous time (240 min). Subsequently, the average value data was calculated for analysis, that is, the hourly and monthly averages for analysis of hourly and monthly variability were calculated. Additionally, owing to the nature of radio sensor observation equipment such as Wind-LIDAR, incorrect measurements often result from atmospheric conditions such as cloud and aerosols affecting backscatter, or data collection rate decreases with increasing altitude, and there are also some periods of missing data due to maintenance (Figure 2). Considering these factors, with 200 m, the altitude of the highest observation layer, as the standard, days on which more than two-thirds of data were secured for 24 hours a day were selected, and other days with a lower proportion of data were excluded from the analysis. The purpose of this study was to analyze the general vertical distribution characteristics of wind in the Bonggae area of Jeju Island using data collected over many years, which was averaged monthly and hourly according to the length of the analysis time. Additionally, considering the characteristics of the Korean Peninsula, which experiences all four seasons, we attempted to examine in detail the diurnal characteristics of vertical winds by comparing the diurnal cycle for each season and mean value.
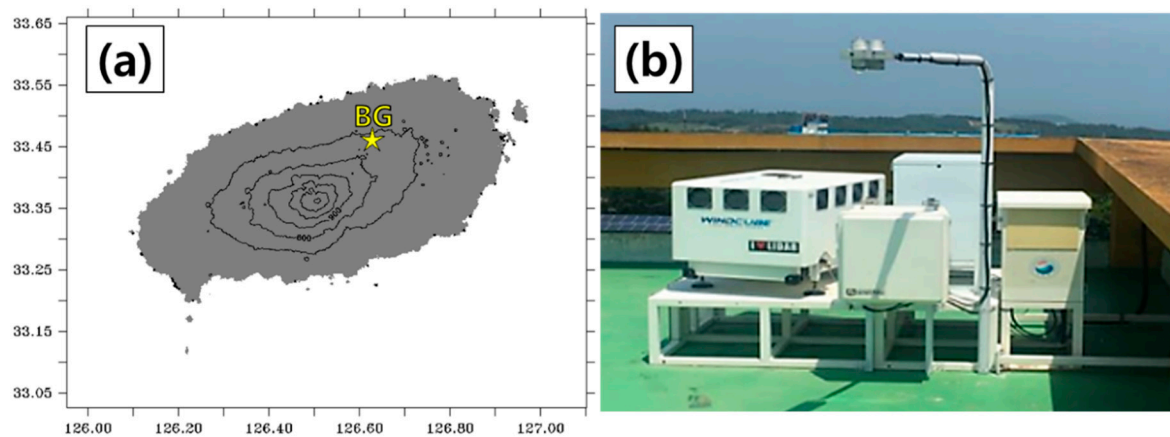
Figure 1. (a) Location (the symbol of yellow star) and (b) Wind-LIDAR installation at Bonggae (BG) station in Jeju Island of South Korea.
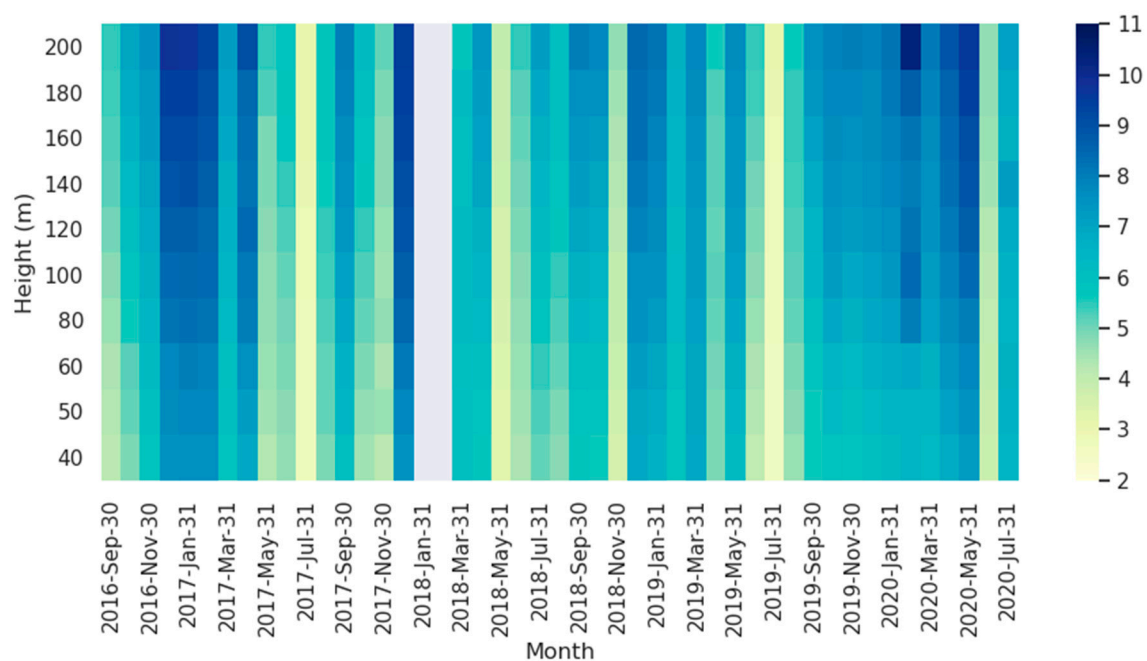

Figure 2. Monthly mean wind speed (ms⁻¹) for multiple levels for Bonggae (BG) station. The shaded color in gray indicates the period of missing data (2018.01.-2018.02.).

3. Results

3.1. Characteristics of Monthly Cycle and Characteristics via Elevation of Bonggae's Wind

The average monthly wind speed in the BG area, where vertical wind was observed for a long period, varied over a range from 2.57 ms⁻¹ to ~10.49 ms⁻¹, and the wind in the upper layer tended to be relatively strong compared with the wind in the lower layer (Figure 2). Additionally, the typical East Asian seasonal wind characteristics, which are relatively weakened in summer and strengthened in winter, were well reflected, particularly in winter, when the upper layer wind was stronger compared with the other seasons. Based on years of observation, the average wind speed from January to December were found to be 7.65 ms⁻¹ on average in the months of December, January, and February (DJF), which correspond to winter, and were relatively larger compared with other seasons (March–April–May, MAM: 6.66 ms⁻¹, September–October–November, SON: 6.21 ms⁻¹). Moreover, in the context of the wind direction, the northwest wind was dominant relative to other seasons (Figure 3). After winter, the northwest wind gradually weakened, and the wind speed gradually decreased;

moreover, in the spring (March to May), the wind direction of the north–south components was dominant and the east–west wind components almost disappeared. In the summer (June to August), the average wind speed was the lowest of the year (4.79 ms^{-1}), and the east wind gradually increased. Subsequently, the east wind quickly changed its direction toward the east–south–west as the fall season (September to November) approached, followed by the arrival of the winter season.
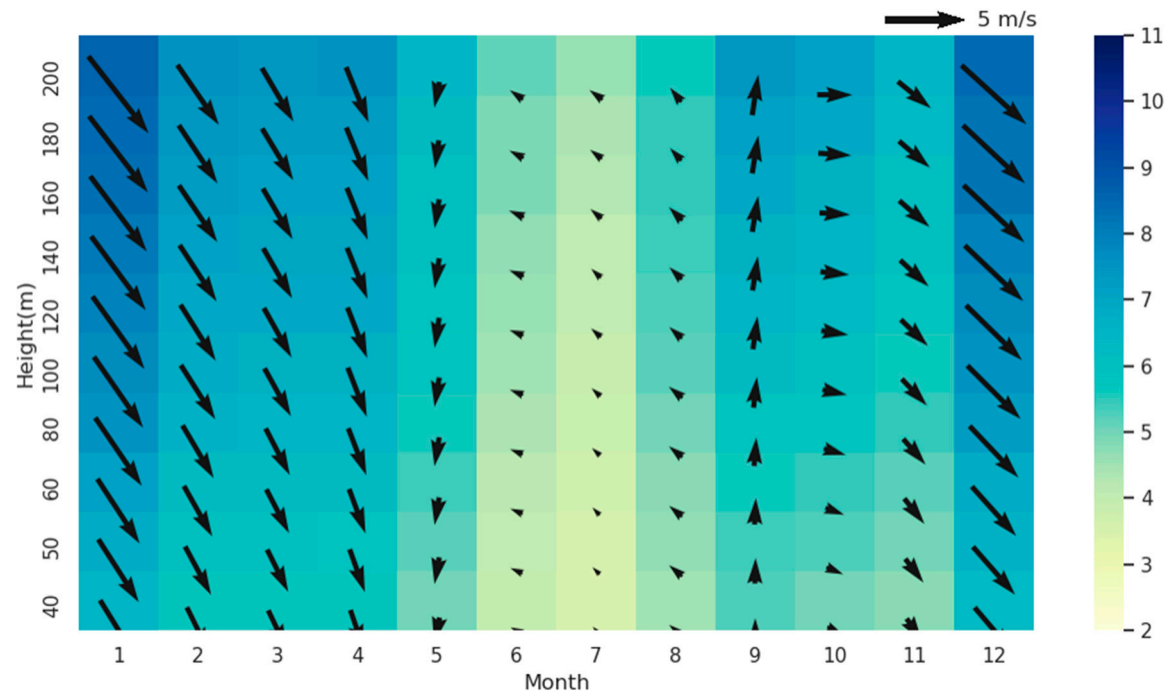

Figure 3. Monthly mean wind speed (ms^{-1}) and wind direction for multiple levels.

As described earlier, wind direction and wind speed in the BG area were highly correlated regardless of altitude, and when the wind was strong, the northwest wind was dominant, whereas when the wind was weak, the southeast wind dominated. Additionally, the characteristic of the clockwise circulation of the wind in all layers was confirmed during the year starting from spring. This means that wind directions at an altitude of 40–200 m in the lower layer have the same variability, suggesting that the influence of the surrounding seasonal winds running lengthwise, including in the observation area, plays a major role. Wind speed characteristics according to altitude were also clearly observed, with 4.91 to 8.76 ms^{-1} in the highest layer of observation altitude and 3.76 to 6.96 ms^{-1} in the lowest layer of observation altitude; moreover, the largest wind speed appeared in the highest layer in December and the smallest wind speed appeared in the lowest layer in July (Table 1). Thus, the monthly wind speed showed a distinct difference depending on the season, and according to altitude, the upper layer was approximately 21.2%–38.6% larger than in the lower layer. Particularly, the reason for the increase in the wind speed in the upper layer during winter is that the influence of ground friction decreases with increasing altitude; moreover, the wind speed increases because it is influenced by the northwest seasonal wind. Additionally, the relatively weak upper layer wind speed in summer is due to weakened horizontal advection as the vertical mixing between upper and lower layers is strengthened by the ground strongly heated by the sun along with the weakened northwest seasonal wind. Moreover, the wind direction associated with horizontal advection is also highly correlated with the wind speed, which can be clearly observed from the average wind speed for each wind direction in the order of north wind (11.0 ms^{-1}), west wind (7.2 ms^{-1}), east wind (6.0 ms^{-1}), and south wind (5.1 ms^{-1}).

Table 1. Monthly mean wind speed (ms⁻¹) for multiple levels averaged for all periods.

(m)	JAN	FEB	MAR	APR	MAY	JUN	JUL	AUG	SEP	OCT	NOV	DEC
200	8.75	7.86	7.64	7.80	6.75	5.39	4.91	5.75	7.56	7.24	6.61	8.76
180	8.59	7.67	7.52	7.53	6.54	5.21	4.68	5.68	7.31	7.08	6.43	8.51
160	8.43	7.55	7.34	7.37	6.35	5.12	4.56	5.66	7.04	6.87	6.29	8.40
140	8.27	7.38	7.21	7.22	6.27	4.96	4.41	5.55	6.87	6.63	6.13	8.20
120	8.07	7.24	7.14	7.10	6.15	4.83	4.33	5.44	6.63	6.41	5.97	7.99
100	7.86	7.22	6.98	6.93	5.98	4.72	4.21	5.33	6.40	6.16	5.81	7.76
80	7.71	7.10	6.84	6.76	5.82	4.61	4.07	5.18	6.12	5.92	5.65	7.56
60	7.36	6.84	6.61	6.50	5.63	4.47	3.95	4.98	5.81	5.63	5.40	7.24
50	7.17	6.67	6.49	6.31	5.47	4.37	3.86	4.88	5.64	5.45	5.28	7.05
40	6.96	6.49	6.30	6.10	5.28	4.25	3.76	4.72	5.52	5.23	5.08	6.84
Mean	7.92	7.20	7.01	6.96	6.03	4.79	4.27	5.32	6.49	6.26	5.87	7.83

3.2. Mean Diurnal Characteristics of Bonggae's Winds

In addition to analyzing the characteristics of monthly variability, diurnal cycles were investigated to determine the characteristics of the vertical wind in a shorter period of time in the Bonggae region. Similar to the strong (weak) wind appearing in winter (summer) in the average daily cycle of vertical winds during the entire period, the wind direction and wind speed were characterized by increasing or decreasing solar radiation (Figure 4). In the case of wind direction, the wind of the north wind group was observed to dominate at all altitudes and all the times; moreover, the wind direction changed to the west wind at ~8 am at the beginning of sunrise in the lower layer and then to the north wind at ~5 pm. In the case of wind speed, periodicity of minimum wind speed appearing at 8 am on average in all vertical layers as well as in the lower layer and the maximum wind speed appearing at 2 pm was observed (Figure 5). To examine this periodicity in more detail, the difference between the daily cycle of wind speed and minimum wind speed at each altitude was calculated to determine the time point during the day when the minimum wind speed appeared (Figure 6). Additionally, through related analysis, determining the relative change in wind speed according to altitude from the time when the minimum wind speed appeared was possible. As with the aforementioned results, the time point of minimum wind speed was 8 am in the 40–80 m section of the lower layer, and 9 am, one hour late in the 100–200 m section. This clearly indicates that there is a time lag of ~1 hour depending on the altitude during the sunrise time. Additionally, there was a high correlation of at least 0.96 or more with the wind speed diurnal cycle at two adjacent altitudes in the upper and lower layers (Table 2), which clearly indicates that at minimum wind speeds, there is also a high correlation relationship among minimum wind speed time. These characteristics are also likely to be related to the surrounding environment of Bonggae, where there are few topographical features affecting wind speed changes.
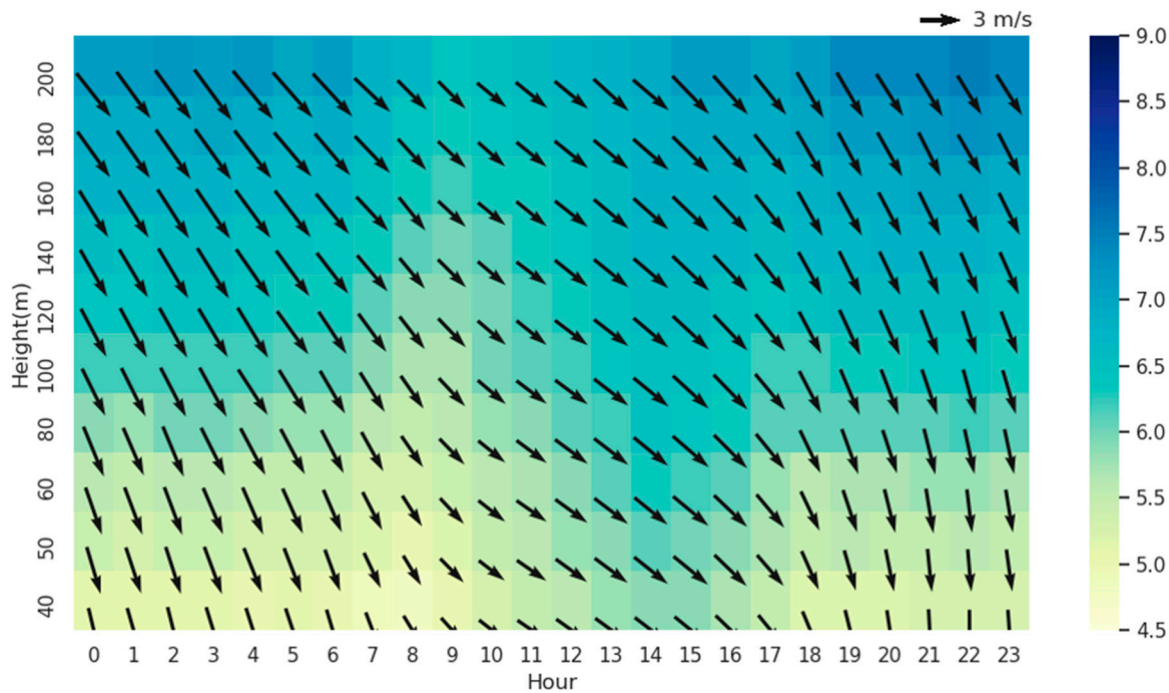
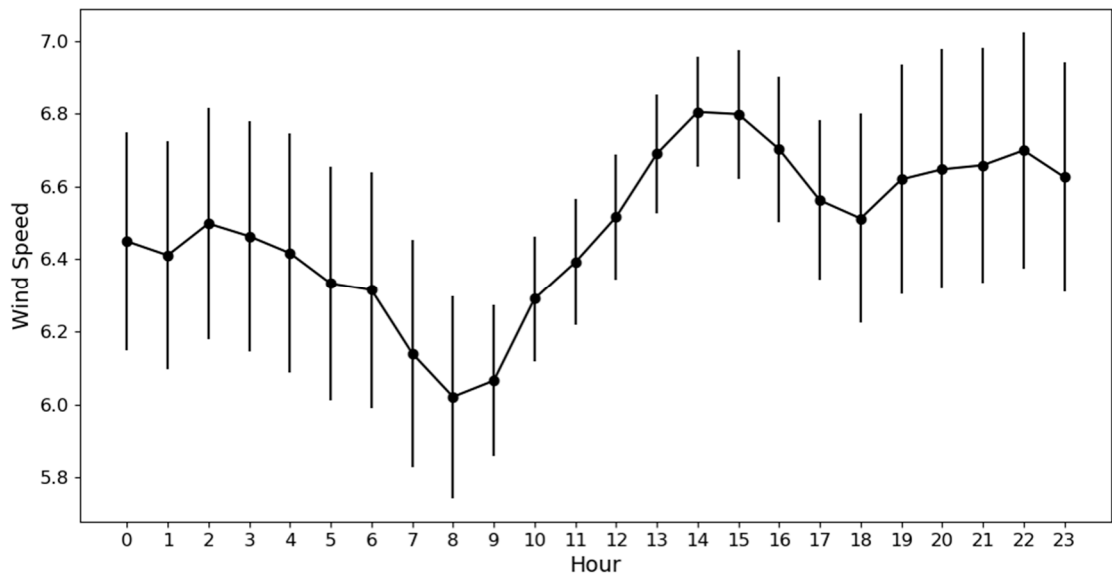**Figure 4.** Diurnal cycle of mean wind speed (ms⁻¹) and wind direction averaged for all periods.

Figure 5. Diurnal mean and standard deviation of wind speed (ms⁻¹) averaged for all altitudes.
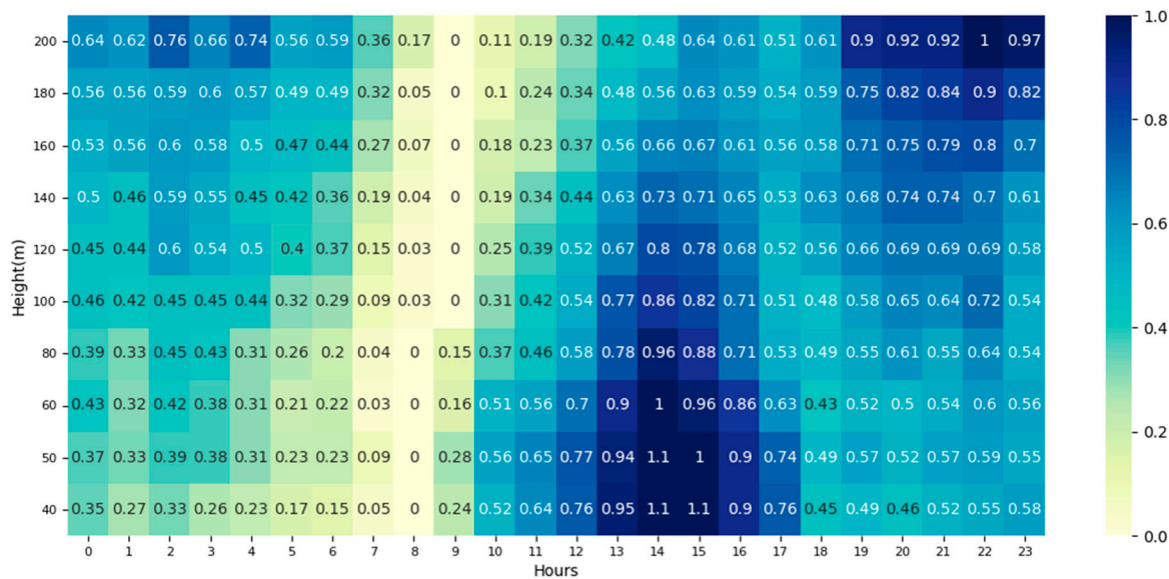
Figure 6. Difference between diurnal mean wind speed (ms⁻¹) and minimum value for each altitude.

Table 2. Correlation coefficients among wind speeds for multiple levels.

Height	40 m	50 m	60 m	80 m	100 m	120 m	140 m	160 m	180 m	200 m
200 m	0.07	0.11	0.21	0.38	0.56	0.71	0.80	0.91	0.97	1.00
180 m	0.27	0.31	0.39	0.55	0.71	0.83	0.90	0.98	1.00	
160 m	0.41	0.45	0.53	0.68	0.82	0.91	0.96	1.00		
140 m	0.59	0.63	0.70	0.82	0.92	0.98	1.00			
120 m	0.70	0.74	0.80	0.89	0.96	1.00				
100 m	0.83	0.86	0.91	0.96	1.00					
80 m	0.93	0.95	0.97	1.00						
60 m	0.98	0.99	1.00							
50 m	0.99	1.00								
40 m	1.00									

3.3. Diurnal Characteristics in each Season of Bonggae Winds

Earlier, the northwest wind was observed to dominate the monthly and daily cycles of the vertical wind, and the characteristics of the wind according to solar radiation were similar to each other (Figures 3 and 4). However, in summer, the east wind dominates in the monthly cycle and the west wind dominates in the diurnal cycle. This suggests that diurnal cycle of the wind differs seasonally. To further investigate this variability, the seasonal characteristics of diurnal cycle were examined; consequently, the main wind direction was different depending on the season (Figure 7), unlike the results of the year-round northwest wind dominating the diurnal cycle mean during the entire period (Figure 4). Same as the average diurnal cycle result, winter was the season when the northwest wind was most dominant, meaning that winter is the most important season for the average annual wind direction in comparison with other seasons (Figure 7d). In winter, the biggest feature was that the northwest wind was continuously maintained regardless of altitude and diurnal cycle. The second strongest north wind season after winter was spring, and the north wind in spring was weak compared with winter by ~29.4% (−4.58 ms⁻¹ → −3.54 ms⁻¹). Moreover, the west wind was weak by more than half (3.47 ms⁻¹ → 1.39 ms⁻¹), and the west wind was briefly strengthened only after the sun was out (Figure 7a).
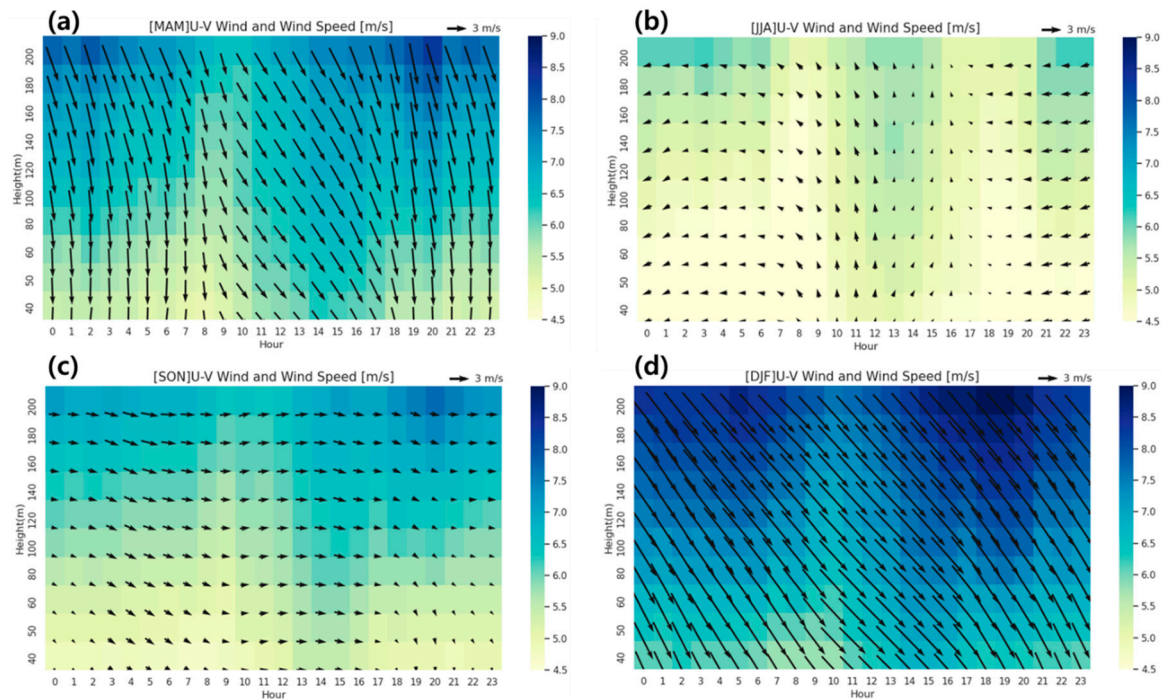
Figure 7. Diurnal cycle of mean wind speed (ms⁻¹) and wind direction averaged for all periods for (a) March–April–May (MAM), (b) June–July–August (JJA), (c) September–October–November (SON), (d) December–January–February (DJF).

During the summer period, the north wind was relatively weakened (-3.54 ms⁻¹ $\rightarrow 0.68$ ms⁻¹) compared with the previous season. Additionally, the east–west wind switched from the west to east wind only in summer, but its value was relatively small compared with other seasons (Figure 7b). This phenomenon occurred because the ground was heated the most by solar radiation in summer compared with other seasons and the influence of horizontal advection flow from the surroundings due to strong vertical mixing decreased. Moreover, the main wind direction changed from east to west, unlike in summer, and the previously weakened west wind gradually strengthened (-0.75 ms⁻¹ $\rightarrow 1.44$ ms⁻¹) (Figures 7b, c). Subsequently, the west wind reached its peak strength in winter. As mentioned earlier, the wind in the Bonggae area of Jeju shows different wind speeds and wind direction characteristics according to the season.

3.4. Maximum Wind Speed Characteristics of Bonggae Wind According to Altitude

Previously, we found that the minimum wind speed at each altitude appeared at 8 to 9 am on average and was delayed by ~1 hour in the upper layer compared with the lower layer (Figure 6). The wind speeds at each altitude were confirmed to be closely related with each other, exhibiting similar variability between adjacent altitudes. However, the correlation of wind speeds at adjacent altitudes weakened as the altitudes were gradually separated farther (Table 2), suggesting that the time lag at each altitude may appear differently. The diurnal wind speed was minimal at 8–9 am on average, and its strength gradually increased as a result of increased vertical mixing owing to ground heating after sunrise. The time when the maximum wind speed was observed, unlike the minimum wind speed, was considerably influenced by lengthwise seasonal winds and ground heating by the sun in each season. To examine this phenomenon in detail, the time of day when the wind speed was maximized at each altitude was compared and analyzed according to season (Figure 8).
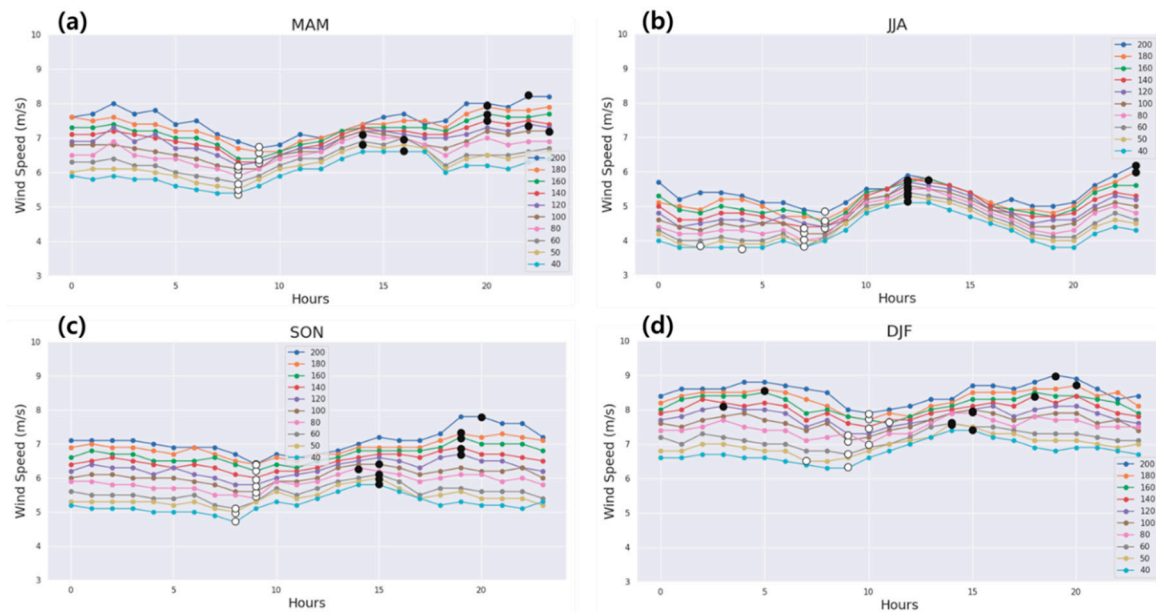
Figure 8. Diurnal means wind speed (ms⁻¹) in multiple levels for (a) March–April–May (MAM), (b) June–July–August (JJA), (c) September–October–November (SON), (d) December–January–February (DJF). The black (white) filled dots indicate the value when the maximum (minimum) wind speed appeared for each level.

A common feature that appeared for all seasons was that the maximum wind speed appeared first in the lowest layer after sunrise and then the maximum wind speed appeared in the upper layer. However, there was a difference in the appearance of delayed maximum wind speed depending on the season. Maximum spring wind speed appeared largely divided into two groups: the first appeared at 2–4 pm in the section at an altitude of 40–80 m, which was approximately half of the lower layer of the observed altitude, and then the second, delayed by ~4 hours, appeared at 8–11 pm in the section at a relatively high altitude of 100–200 m (Figure 8a). As mentioned earlier, the fact that the maximum wind speed at each altitude occurs at different time points means that the wind speed at each altitude is determined differently. In the lower layer, the wind speed gradually increased after sunrise to reach the maximum at ~3 pm, and then decreased with decreasing vertical mixing. However, in the upper layer with relatively strong wind, the wind speed that decreased after sunrise gradually increased again and continued to increase even after sunset, which resulted in the maximum wind speed appearing at night. As mentioned earlier, the maximum speed of the spring wind exhibited a time lag between the lower and upper layers owing to vertical mixing associated with the diurnal cycle of solar radiation. The fall also showed similar results to the spring, with the maximum wind speed appearing at 40–140 m in the lower layer at approximately 2–3 pm, and then at 120–200 m at 7–8 pm, delayed by ~4 hours (Figure 8c).

The summer showed considerably different results from the previous two seasons; basically, the average wind speed was relatively small at all times and variability among altitudes was also the smallest (Figure 8b). Particularly, the variability among altitudes was minimal at ~11 am after sunrise, and the maximum wind speed appeared in all sections of 40–160 m except for the top two layers at 12–1 pm. Thus, the relatively small diurnal variability of the wind speed in summer compared with other seasons and the occurrence of the maximum wind speed were almost simultaneously correlated to vertical mixing by overwhelmingly strong solar radiation. Additionally, in summer, the influence of the wind running lengthwise was small and the distance between the earth and sun was minimal. Consequently, the appearance of maximum wind speed in the upper layer was also delayed by 10 hours in the 180–200 m section. However, in winter, the average wind speed was relatively higher than other seasons, unlike summer, and the biggest feature was that the time when the maximum wind speed appeared to be distributed at various times (Figure 8d). Although the maximum wind

speed first appeared in the 40–100 m section at 2–3 pm after sunrise, nonlinear characteristics appeared regardless of delay, such as at 6 pm, 7 pm, and 8 pm, and at 3 am and 5 am, at higher altitudes. This was mainly due to the influence of the northwest seasonal wind, which becomes stronger in winter, rather than the influence of solar radiation. Additionally, these characteristics appeared similarly in the hours of day when the minimum wind speed at each altitude appeared, with a constant delay of ~1 hour between the upper and lower layers in spring and autumn, a long delay of ~6 hours in summer, and some delay in winter, but with irregularities among altitudes.

3.5. Long-term Tendency of Bonggae's Wind

From the results of approximately five-year observation in Bonggae, we found that the wind speed exhibited an increasing tendency (Figure 9). Wind speed data at four adjacent automated weather station (AWS) points (Table 3) was compared to confirm whether these characteristics were limited to one area, and the same increasing trend was also observed. Nevertheless, because the tendency in this long period from a climatic perspective may be a natural variability, the AWS analysis period was extended back to the year 2000 to examine wind speed variability for a total of 20 years (Figure 10). Though there was increase or decrease depending on the year, the wind speed had been steadily decreasing from about 2004 to 2016, and these results have also been presented in global trend analysis using ddthe Coupled Model Intercomparison Project (CMIP6) [27] and East Asian studies using observation data [28–31]. Since then, though there have been differences in time depending on the analysis area, the wind speed has changed again around 2016 [30,31](Liu et al., 2018; Kim and Paik., 2015), which is consistent with the results at Bonggae and AWS. This means properly understanding the long-term tendency of wind speeds not only for location selection and power generation calculation of wind power generation complexes but also for their long-term operation is crucial [32–35]. Furthermore, expansion of observation and operation using Wind-LIDAR to a wider area in the future is essential.
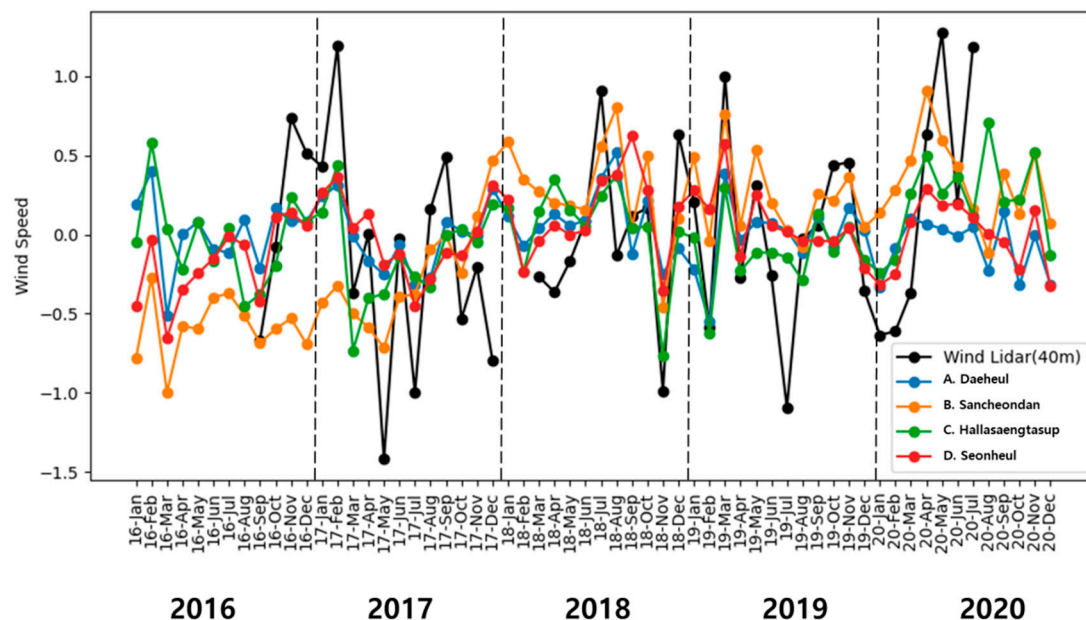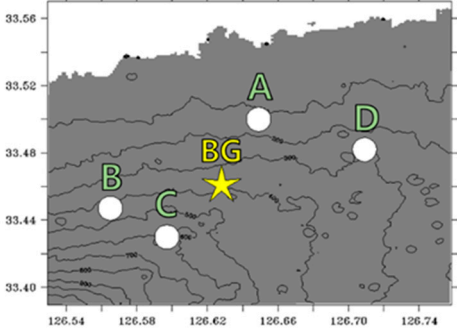

Figure 9. Monthly variability of wind speed (ms⁻¹) for Wind-LIDAR at 40 m at Bonggae (BG) station and automated weather stations around BG station.

Table 3. Basic information of automated weather station around Bonggae (BG) station.

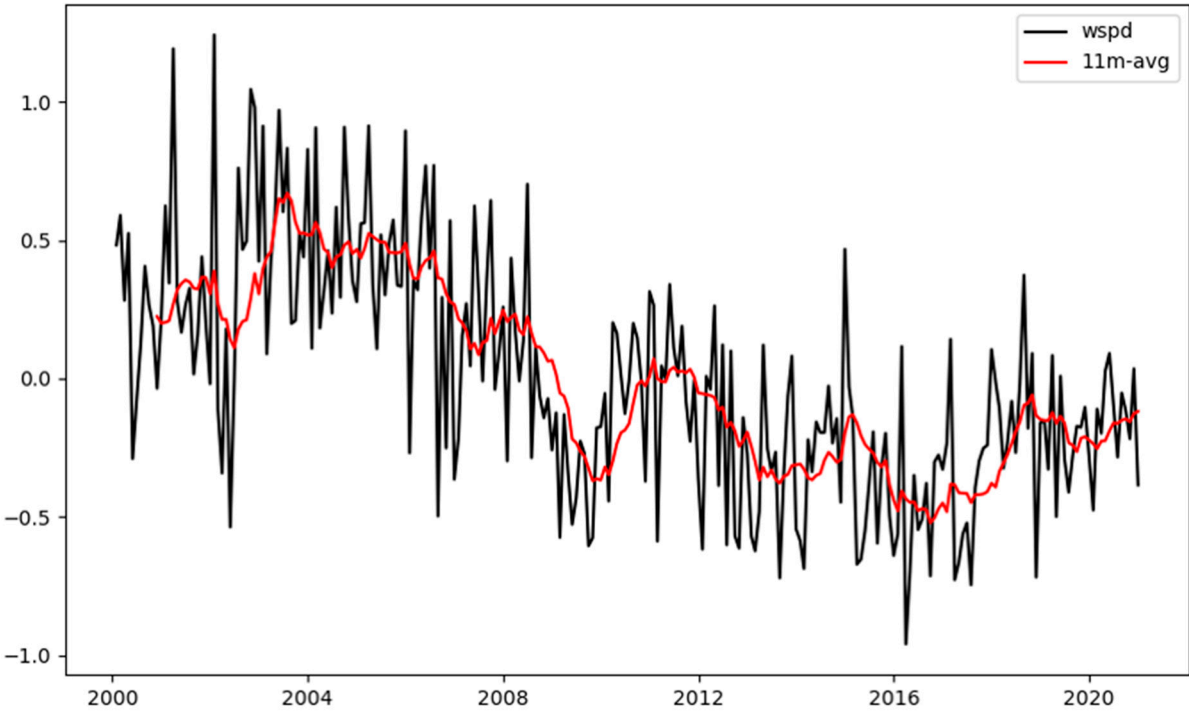| #	Name	Latitude (°N)	Longitude (°E)
A	Daeheul	33.447336	126.56546
B	Sancheondan	33.50081	126.64947
C	Hallasaengtaes up	33.43023	126.59777
D	Seonheul	33.48209	126.70904

Figure 10. Monthly variability of wind speed (ms⁻¹) averaged for automated weather stations around Bonggae station. The red line indicates 11-month running mean.

4. Summary and Discussion

Herein, we investigated the monthly cycle and diurnal characteristics of vertical winds in the Bonggae area of Jeju Island and confirmed the characteristics of variability below and above SL, which belongs to the lower layer of ABL. For monthly cycle, the wind speed weakened/strengthened in summer/winter, and the wind direction was dominated by northwest wind in winter and by the east wind in summer, but the amplitude of the wind speed in summer was relatively small. We could confirm that these characteristics were consistent at all altitudes and closely correlated with each other by altitude. These characteristics appeared similarly in the diurnal wind speed, and there was generally a characteristic delay of ~1 hour between the upper and lower layers. These characteristic delays differed according to the season, with spring and autumn exhibiting a division between the upper and lower layers showing consistent characteristics, whereas in summer, the maximum wind speed appeared simultaneously for ~10 hours earlier in all lower layers except for some of the upper layers. This seems to be owing to the relatively strong solar radiation and active vertical mixing. In winter, the maximum wind speed was nonlinear; therefore, the delay characteristics between altitudes did not appear, which was owing to the influence of the nearby strong northwest seasonal

winds, contrary to summer. Additionally, the wind speed exhibited a long-term increasing tendency, which is consistent with previously known research results and adjacent AWS results.

These research results are expected to contribute to providing information that can be used as an important indicator concerning the power generation efficiency of renewable energy such as wind power generation within SL and energy production industry. Additionally, through this study, extending the wind characteristics at ground observation and wind power generation altitudes to a study based on observation, away from the existing similarity theory, is essential. A previous study suggested the effect of atmospheric stability on the efficiency of wind power generation complex and demonstrated that there was no difference in stability due to low power generation below a specific wind speed [36].

Furthermore, in a recent study on Urban Air Mobility (UAM) [37,38], Vertiport, where UAM actually takes off and lands, belong to an altitude sensitive to the influence of the inertial and roughness sublayers within SL; therefore, we expect our current study to be utilized for safe operation of UAM.

Author Contributions: Conceptualization, D.-W.Y. and S.-S.L.; methodology, D.-W.Y., S.-S.L. and H.-W.C.; software, D.-W.Y..; validation, D.-W.Y., S-S.L. and H.-W.C.; formal analysis, D.-W.Y. and S.-S.L.; investigation, Y.H.L.; resources, D.-W.Y.; data curation, D.-W.Y.; writing—original draft preparation, D.-W.Y.; writing—review and editing, all authors; visualization, D.-W.Y.; supervision, S.-S.L.; project administration, Y.H.L.; funding acquisition, Y.H.L. All authors have read and agreed to the published version of the manuscript.

Institutional Review Board Statement: "Not applicable".

Informed Consent Statement: "Not applicable.".

Data Availability Statement: The wind-LIDAR data obtained from the National Institute of Meteorological Sciences. The datasets of automatic weather stations (AWSs) used in this study are publicly available in the archives: https://data.kma.go.kr.

Conflicts of Interest: The authors declare no conflict of interest.

References

1. Rhodes, C.J. The 2015 Paris Climate Change Conference: COP21. Sci. Prog. 2016, 99, 97-104; DOI:10.3184/003685016X14528569315192.
2. Macknick, J.; Newmark, R.; Heath, G.; Hallett, K.C. Operational Water Consumption and Withdrawal Factors for Electricity Generating Technologies: A Review of Existing Literature. Environ. Res. Lett. 2012, 7, 45802; DOI:10.1088/1748-9326/7/4/045802.
3. Boyle, G. Renewable Energy; Oxford University Press: Oxford, UK, 2004.
4. Stull, R.B. An Introduction to Boundary Layer Meteorology; Springer Science; Business & Media: London, UK, 1988; Vol. 13, p 187. DOI:10.1007/978-94-009-3027-8.
5. Porté-Agel, F.; Lu, H.; Wu, Y.T. Interaction Between Large Wind Farms and the Atmospheric Boundary Layer. Proced. Lutam. 2014, 10, 307-318; DOI:10.1016/j.piutam.2014.01.026.
6. National Academies of Sciences. Engineering, and Medicine Thriving on Our Changing Planet: A Decadal Strategy for Earth Observation from Space; National Academies Press: Washington, DC. 2018a. DOI:10.17226/24938.
7. National Academies of Sciences. Engineering, and Medicine. The Future of Atmospheric Boundary Layer Observing, Understanding, and Modeling. Proc. Workshop; National Academies Press: Washington, DC. 2018b. DOI:10.17226/25138.
8. Goodess, C.M.; Troccoli, A.; Acton, C.; Añel, J.A.; Bett, P.E.; Brayshaw, D.J.; De Felice, M.; Dorling, S.R.; Dubus, L.; Penny, L.; Percy, B.; Ranchin, T.; Thomas, C.; Trolliet, M.; Wald, L. Advancing Climate Services for the European Renewable Energy Sector Through Capacity Building and User Engagement. Clim. Serv. 2019, 16, 100139; DOI:10.1016/j.cliser.2019.100139.
9. St Martin, C.M.; Lundquist, J.K.; Clifton, A.; Poulos, G.S.; Schreck, S.J. Wind Turbine Power Production and Annual Energy Production Depend on Atmospheric Stability and Turbulence. Wind Energ. Sci. 2016, 1, 221-236; DOI:10.5194/wes-1-221-2016.

10. Doörenkaämper, M.; Tambke, J.; Steinfeld, G.; Heinemann, D.; Kühn, M. Atmospheric Impacts on Power Curves of Multi-Megawatt Offshore Wind Turbines. J. Phys. Conf. S. 2014, 555, 012029; DOI:10.1088/1742-6596/555/1/012029.

11. Wharton, S.; Lundquist, J.K. Atmospheric Stability Affects Wind Turbine Power Collection. Environ. Res. Lett. 2012, 7, 014005; DOI:10.1088/1748-9326/7/1/014005.

12. Antoniou, I.; Pedersen, S.M.; Enevoldsen, P. B. Wind Shear and Uncertainties in Power Curve Measurement and Wind Resources. Wind Eng. 2009, 33, 449-468; DOI:10.1260/030952409790291208.

13. Kashani, A.G.; Olsen, M.J.; Parrish, C.E.; Wilson, N. A Review of Lidar Radiometric Processing: From AD HOC Intensity Correction to Rigorous Radiometric Calibration. Sensors 2015, 15, 28099-28128; DOI:10.3390/s151128099.

14. Emeis, S.; Harris, M.; Banta, R.M. Boundary-layer Anemometry by Optical Remote Sensing for Wind Energy Applications. Meteorologische, 2007, 16.4, 337-348; DOI:10.1127/0941-2948/2007/0225.

15. Weitkamp, C. Lidar Range-Resolved Optical Remote Sensing of the Atmosphere; In Springer Series in Optical Sciences; Springer: Singapore, 2005; Vol. 102, p 40. DOI:10.1007/b106786.

16. Melfi, S.H.; Lawrence, J.D.; McCormick, M.P. Observation of Raman Scattering by Water Vapor in the Atmosphere. Appl. Phys. Lett. 1969, 15, 295-297; DOI:10.1063/1.1653005.

17. Cooney, J.A. Measurements on the Raman Component of Laser Atmospheric Backscatter. Appl. Phys. Lett. 1968, 12, 40-42; DOI:10.1063/1.1651884.

18. Schotland, R.M. Some Observations of the Vertical Profile of Water Vapor by a laser Optical Radar. In Proc. 4th Symposium on Remote Sensing of Environment, Ann Arbor: University of Michigan, 1966; Vol. 12-14, p 273-283.

19. Smullin, L.D.; Fiocco, G. Optical Echoes from the Moon. Nature 1962, 194, 1267; DOI:10.1038/1941267a0.

20. Woodbury, E.J.; Congleton, R.S.; Morse, J.H.; Stitch, M.L. Design and Operation of an Experimental Colidar; IRE WESCON Convention: California, USA, 1961; Vol. 24.

21. Maiman, T.H. Stimulated Optical Radiation in Ruby. Nature 1960, 187, 493-494; DOI:10.1038/187493a0.

22. Gonzalez-Aparicio, I.; Monforti, F.; Volker, P.; Zucker, A.; Careri, F.; Huld, T.; Badger, J. Simulating European Wind Power Generation Applying Statistical Downscaling to Reanalysis Data. Appl. Energy 2017, 199, 155-168; DOI:10.1016/j.apenergy.2017.04.066.

23. Liu, Z.; Barlow, J.F.; Chan, P.W.; Fung, J.C.H.; Li, Y.; Ren, C.; Mak, H.W.L.; Ng, E. A Review of Progress and Applications of Pulsed Doppler Wind LiDARs. Remote Sens. 2019, 11, 2522; DOI:10.3390/rs11212522.

24. Fujii, T.; Fukuchi, T. Laser Remote Sensing (1st ed.); CRC Press: Boca Raton, FL, USA, 2005. DOI:10.1201/9781420030754.

25. Kim, H.G.; Chyng, C.W.; An, H.J.; Ji, Y.M. Comparative Validation of Windcube LIDAR and Remtech SODAR for Wind Resource Assessment - Remote Sensing Campaign at Pohang Accelerator Laboratory. J. Korean Sol. Energy Soc. 2011, 31, 63-71; DOI:10.7836/kses.2011.31.2.063.

26. Korea Meteorological Administration. Meteorological Observation Standardization Manual, Republic of Korea, 2019. 11-1360000-001611-09.

27. O'Neill, B.C.; Tebaldi, C.; Van Vuuren, D.P.; Eyring, V.; Friedlingstein, P.; Hurtt, G.; Knutti, R.; Kriegler, E.; Lamarque, J.F.; Lowe, J.; Meehl, G.A. The Scenario Model Intercomparison Project (ScenarioMIP) for CMIP6. Geosci. Model Dev. 2016, 9, 3461-3482; DOI:10.5194/gmd-9-3461-2016.

28. Zha, J.; Shen, C.; Zhao, D.; Wu, J.; Fan, W. Slowdown and Reversal of Terrestrial Near-Surface Wind Speed and Its Future Changes over Eastern China. Environ. Res. Lett. 2021, 16, 034028; DOI:10.1088/1748-9326/abe2cd.

29. Shen, C.; Zha, J.; Zhao, D.; Wu, J.; Fan, W.; Yang, M.; Li, Z. Estimating Centennial-Scale Changes in Global Terrestrial Near-Surface Wind Speed Based on CMIP6 GCMs. Environ. Res. Lett. 2021, 16, 084039; DOI:10.1088/1748-9326/ac1378.

30. Liu, J.; Gao, Z.; Wang, L.; Li, Y.; Gao, C.Y. The Impact of Urbanization on Wind Speed and Surface Aerodynamic Characteristics in Beijing during 1991–2011. Meteorol. Atmos. Phys. 2018, 130, 311-324; DOI:10.1007/s00703-017-0519-8.

31. Kim, J.C.; Paik, K. Recent Recovery of Surface Wind Speed After Decadal Decrease: A Focus on South Korea. Clim. Dyn. 2015, 45, 1699-1712; DOI:10.1007/s00382-015-2546-9.

32. Adams, A.S.; Keith, D.W. Are Global Wind Power Resource Estimates Overstated? Environ. Res. Lett. 2013, 8, 015021; DOI:10.1088/1748-9326/8/1/015021.

33. Kim, H.G. Preliminary Estimation of Wind Resource Potential in South Korea. J. Korean Sol. Energy Soc. 2008, 28, 1-12; DOI:10.7836/kses.2016.36.6.001.

34. Baidya Roy, S.; Pacala, S.W.; Walko, R.L. Can Large Wind Farms Affect Local Meteorology? J. Geophys. Res. 2004, 109, D19; DOI;10.1029/2004JD004763.

35. Keith, D. W.; DeCarolis, J.F.; Denkenberger, D.C.; Lenschow, D.H.; Malyshev, S.L.; Pacala, S.; Rasch P.J. The Influence of Large-Scale Wind Power on Global Climate. Proc. Natl Acad. Sci. U. S. A. 2004, 101, 16115-16120; DOI:10.1073/pnas.0406930101.

14

36. Jeong, H.S.; Kim, Y.H.; Choi, H.W. Characteristics of Wind Environment in Dongbok Bukchon Wind Farm on Jeju. New Renew. Ener. 2022, 18, 1-16; DOI:doi.org/10.7849/ksnre.2022.2027.

37. Steiner, M. Urban Air Mobility: Opportunities for the Weather Community. Bull. Am. Meteorol. Soc. 2019, 100(11), 2131-2133; DOI:10.1175/BAMS-D-19-0148.1.

38. Reiche, C.; McGillen, C.; Siegel, J.; Brody, F. Are We Ready to Weather Urban Air Mobility (UAM)?. In 2019 Integrated Communications, Navigation and Surveillance Conference (ICNS); Herndon: VA, USA, 2019, p 1-7, DOI:10.1109/ICNSURV.2019.8735297.